Rapid Methods for Radionuclide Contaminant Transport in Nuclear Fuel Cycle Simulation

Kathryn Huff[a]

[a]*Department of Nuclear, Plasma, and Radiological Engineering, 118 Talbot Laboratory, MC 234, University of Illinois at Urbana-Champaign, Urbana, IL 61801*

Abstract

Nuclear fuel cycle and and nuclear waste disposal decisions are technologically coupled. However, current nuclear fuel cycle simulators lack dynamic repository performance analysis due to the computational burden of high-fidelity hydrolgic contaminant transport models. The Cyder disposal environment and repository module was developed to fill this gap. It implements medium-fidelity hydrologic radionuclide transport models to support assessment appropriate for fuel cycle simulation in the Cyclus fuel cycle simulator.

Rapid modeling of hundreds of discrete waste packages in a geologic environment is enabled within this module by a suite of four closed form models for advective, dispersive, coupled, and idealized contaminant transport: a Degradation Rate model, a Mixed Cell model, a Lumped Parameter model, and a 1-D Permeable Porous Medium model. A summary of the Cyder module, its timestepping algorithm, and the mathematical models implemented within it are presented. Additionally, parametric demonstrations simulations performed with Cyder are presented and shown to demonstrate functional agreement with parametric simulations conducted in a standalone hydrologic transport model, the Clay Generic Disposal System Model developed by the Used Fuel Disposition Campaign Department of Energy Office of Nuclear Energy.

Keywords:
Nuclear fuel cycle, repository, simulation, hydrologic contaminant transport.

1. Introduction

Repository performance metrics provide an important basis for comparison among potential nuclear fuel cycles. Additionally, nuclear fuel cycle and nuclear waste disposal decisions are technologically coupled through the characteristics of spent fuel which vary among fuel cycles and impact repository design and performance (i.e. spent nuclear fuel (SNF) volume, isotopic composition, mass, disposition, and other variables). For this reason, dynamic integration of a

Email address: kdhuff@illinois.edu (Kathryn Huff)

generic disposal model with a fuel cycle systems analysis framework is necessary to illuminate performance distinctions of candidate repository host media, designs, and engineering components in the context of fuel cycle options. However, the computational burden of robust repository performance analysis has previously not been compatible with fuel cycle simulation. Therefore, current nuclear fuel cycle simulators lack coupled repository performance analysis capabilities.

Most current tools treat the waste disposal phase of fuel cycle analysis statically in post processing by reporting values such as mass, volumes, radiotoxicity, or heat production of accumulated SNF and high level waste (HLW). Such tools (e.g., Nuclear Waste Assessment System for Technical Evaluation (NUWASTE) [1], Dynamic Analysis of Nuclear Energy System Strategies (DANESS) [2], Nuclear Fuel Cycle Simulator (NFCSim) [3], and ORION [4]) fail to address the dynamic impact of those waste streams on the performance of the geologic disposal system [5]. Two tools, Commelini-Sicard (COSI) [6] and the Verifiable Fuel Cycle Simulation Model (VISION) [7, 5, 8, 6], dynamically perform heat based capacity calculations. However, those calculations are applicable only for specific repository concepts and cannot inform sensitivity to alternate geologic disposal system characteristics. Since repository capacity and loading strategies are impacted by SNF characteristics such as volume and composition, and since those may vary according to fuel cycle strategy and may over time in scenarios which include transitions between fuel cycles, a dynamic coupling between fuel cycle analysis and repository loading and performance more accurately captures reality.

This paper presents the Cyder software library [9] and its radionuclide contaminant transport models, which were developed to fill this capability gap. To enable dynamic analysis of waste metrics, Cyder provides medium fidelity models to conduct repository performance analysis on efficient timescales appropriate for fuel cycle analyses. It has been implemented as a Facility compatible with version 0.3 of the Cyclus framework [10], but since it is compiled as a dynamically loadable shared object library with a well defined application programming interface (API), it can also be used as a standalone library. An overview of the Cyder framework and mathematical descriptions of its radionuclide transport models appear in Section 2.

The present work also verifies the hydrologic modeling capability in Cyder through parametric simulations performed with Cyder within Cyclus. Those results are presented in Section 3 alongside comparable parametric simulations conducted using a more detailed computational model, the Clay Generic Disposal System Model (GDSM). The Clay GDSM was developed by the Used Fuel Disposition (UFD) Campaign within the Department of Energy (DOE) Office of Nuclear Energy [11] and relies on the GoldSim simulation environment [12] and its contaminant transport module [12].

2. Radionuclide Mass Transport In Cyder

Cyder conducts radionuclide contaminant transport through a generic geologic repository concept to determine the contaminants expected to reach the environment. This calculation informs repository containment and environmental impact performance assesment metrics.

To acheive this, Cyder represents engineered and natural containment barriers as distinct control volumes. These *components* are arranged in a regular grid at a single vertical depth within a geologic component as in Figure 1.

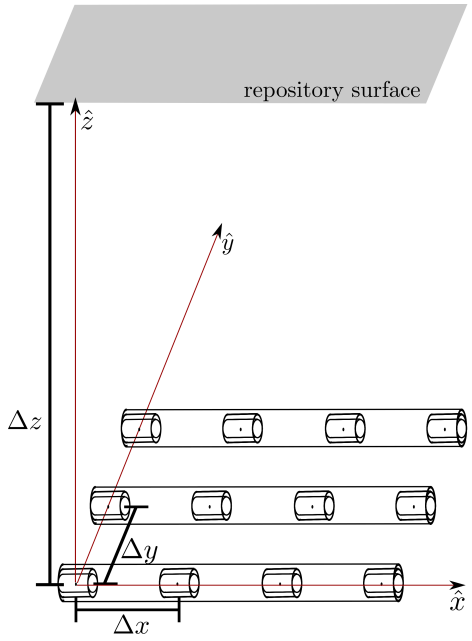

Figure 1: In Cyder, as in a canonical drift-tunnel repository, waste form components (the innermost components) are contained by waste package components which are, in turn, emplaced in a buffer component (the backfilled emplacement tunnel into which waste packages are loaded). That buffer component contains many other waste packages, spaced evenly in a horizontal grid. The geosphere (the outermost component) occupies all space below the repository surface and outside of the buffer components (emplacement tunnels). The Cyder repository layout has a depth (Δz) and package spacing defined by the user input (Δx within the drifts and Δy between drifts.)

Component mass inventory is a simple sum of in and out flows while mass distribution within the component is determined by the dominant physics of the mass balance model selected for that volume. Adjacent components share mass transfer interfaces across which mass transfer is calculated based on internal component mass inventory and distribution.

In Cyder, the mass transfer and mass balance solution follows an implicit *time stepping algorithm*. The solution behavior is determined by selecting

among *mass balance models* within the components and selecting among *mass transfer modes* at boundaries between them. This section will describe the mathematics behind these three aspects of the CYDER paradigm, beginning with the phases of the time stepping algorithm.

2.1. Time Stepping Algorithm

In CYDER, radionuclide contaminants flow outward from the central component, usually the waste form. An implicit time stepping method arrives at the updated state of each component, radially outward, as a function of both the past state and the current state of the system. Mass balance is conducted in each component at each time step. These calculations proceed from the innermost component (e.g. the waste form) to the outermost component (e.g. the far field), with mass transfer calculations conducted at the boundaries. As mass flows from inner components to outer components, the mass balances in both components are updated. Thus, nuclide release information passes radially outward from the waste stream sequentially through each containment layer to the geosphere in a generic geometry of the form in Figure 1. The default timestep in CYCLUS, and therefore in CYDER, is one month.

At each component interface where mass transfer occurs and within each component where mass balances take place, the flow model is solved with the most up to date information available. To illustrate the algorithm by which mass flow calculations are conducted through the system of components at each time step, the phases of a single time step for a simple pair of components will be described.

The flow of the timestepping algorithm is seen in Figures 2, 3, and 4 and is detailed further in the following sections. For the remaining discussion, the source of material, i, is the inner component (i.e. the waste form) and the next destination of the material, j, is the adjacent outer component (i.e. the waste package). This example will be carried through the explanation of all five phases of the timestepping algorithm.

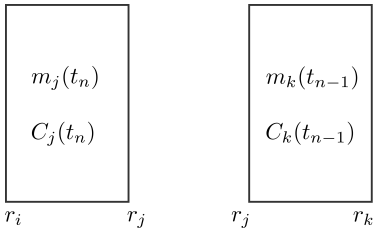

Figure 2: Two components (j and k) share an interface at r_j. They each contain mass (m) and concentration (C) profiles at the beginning of timestep t_n.

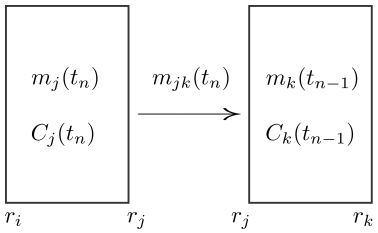

Figure 3: The mass balance model in component (k) calculates the appropriate mass transfer (m_{jk}) based on boundary information from component j.

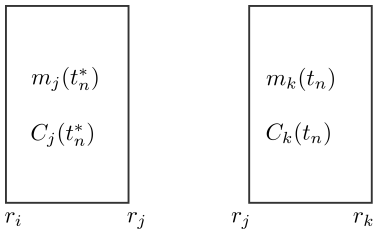

Figure 4: Based on the mass transfer (m_{jk}), both components (j and k) update their mass (m) and concentration (C) profiles based on their respective mass balance models. The asterisk indicates the update correction in the case of the inner component.

2.1.1. Phase 1: Initial Conditions

At the beginning of a timestep, the initial conditions in both the source and the sink are equal to the final updated state of the previous time step. On the first time step, initial mass inventories of each component in the repository system must be defined. In the example case of the source and sink, this might be

$$m_i(t_0) = 10[\text{kg}] \tag{1}$$
$$m_j(t_0) = 0. \tag{2}$$

2.1.2. Phase 2: Interior Mass Balance

The mass distribution, $m_i(\vec{r})$, and concentration profile, $C_i(\vec{r})$, in the interior source volume i at time t_n are calculated based on the initial condition, any influxes, and the physics of its mass balance model. The four different mathematical models available for this mass distribution and concentration profile calculation are discussed in Section 2.2.

The resulting mass distribution and concentration profiles fully inform the conditions on the boundary at r_i. This information is made available to the external component, j in order to support the next phase, the mass transfer calculation. In the example case of the source and sink, this step defines the concentration profile across each volume,

$$C_i(r) = f(r)C_j(r) = 0 \tag{3}$$

where

$$\int f(r)dV = 10. \tag{4}$$

2.1.3. Phase 3: Mass Transfer Calculation

The mass transfer, $m_{ij}(t_n)$ from the source volume i to the sink volume j is calculated next, based on the up to date conditions in volume i (where $0 \leq r \leq r_i$) determined in Phase 2 and the initial conditions in volume j (where $r_i \leq r \leq r_j$). The mass transfer is calculated according to the mass transfer mode preference of the mass balance model of volume j, as discussed in Section 2.3.

In the example case of the source and sink, mass transfered from i to j is determined based on conditions in i and the mass transfer mode between i and j. Said another way, the mass transfer rate m_{ij} between i and j is equivalent to the time derivative $\dot{m}$ of the mass released from i and simultaneously entering j,

$$m_{ij} = -\dot{m}_i = \dot{m}_j. \tag{5}$$

2.1.4. Phase 4: Exterior Mass Balance

When a mass flux m_{ij} is determined between volumes i and j, the mass is added to the exterior sink volume j. Accordingly, necessary updates are made to the mass balance and concentration profile as discussed in Section 2.2. In the case of the source and sink, the mass change in phase 3 is added to the external component, j,

$$m_j(t_n) = m_j(t_{n-1}) + \int_{t_{n-1}}^{t_n} m_{ij}dt \tag{6}$$

$$= m_j(t_{n-1}) + m_{ij}(t_n). \tag{7}$$

2.1.5. Phase 5: Interior Mass Balance Update

When a mass flux $m_{ij}(t_n)$ is determined between volumes i and j, and the mass added to the exterior sink volume j (as in phase 4) it is also extracted from the interior source volume i. When the material is extracted from the interior source volume, the contained mass distribution and concentration profile are updated to reflect this change,

$$m_i(t_n^*) = m_i(t_n) - m_{ij}(t_n). \tag{8}$$

2.2. Mass Balance Models

CYDER tracks the transport of disposed contaminant masses from the innermost component to the outermost far field component and calculates releases to the human biosphere (outside the outermost component) in order to assess containment performance. Accordingly, it is necessary to calculate a mass balance in each component. The four models implemented to assess mass balance are discussed in this section.

The mass balance models selected to represent the physics of mass distribution within each component are selected from among four options. The Degradation Rate model and Mixed Cell model are control volumes that distribute contaminants between a liquid and a solid phase. These models calcuate a homogenous concentration profile throughout the volume and are therefore 0-dimensional in space. The Lumped Parameter model and the One Dimensional Permeable Porous Medium model, however, calculate one dimensional concentration profiles to arrive at a mass distribution throughout the volume.

These models are differentiated from one another by the physics that they capture as well as the detail and accuracy with which they capture it. Depending on the component being modeled, available data, need for accuracy, and need for speed, some mass balance models will be more appropriate than others for certain simulations. This section will provide an overview of these mathematical models and will provide guidance for their appropriate use.

2.2.1. Degradation Rate Radionuclide Mass Balance Model

Barrier materials in a repository environment can degrade very slowly over long time scales. The Degradation Rate mass balance model is the simplest implemented model and is most appropriate for rate based modeling of a degrading barrier volume. The Degradation Rate mass balance model does not attempt to model the physical mechanisms responsible for this degradation. Rather, it generically captures this behavior as a simple fractional degradation rate. The fundamental concept is depicted in Figure 5.

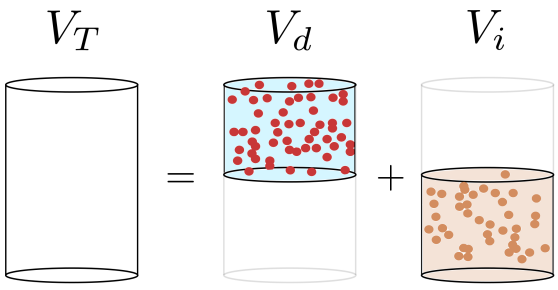

Figure 5: The total control volume (V_T) contains an intact volume (V_i) and a degraded volume (V_d). Contaminants in V_d are available for transport, while contaminants in V_i are contained.

For a situation as in CYDER and CYCLUS, with discrete time steps, the time steps are assumed to be small enough to assume a constant rate of degradation

over the course of the time step. The degraded volume, then, is a simple fraction, d, of the total volume, V_T, such that

$$V_T = V_i + V_d \tag{9}$$

where

$$\begin{aligned} V_d(t) &= d(t)V_T \\ V_i(t) &= (1 - d(t))V_T \\ V_T &= \text{ total volume } [m^3] \\ V_i(t) &= \text{ intact volume at time t } [m^3] \\ V_d(t) &= \text{ degraded volume at time t } [m^3] \end{aligned}$$

and

$$\begin{aligned} d(t) &= \text{ the fraction that has been degraded by time t } [-] \\ &= \sum_{n=0}^{N} f_n \Delta t \end{aligned}$$

where

$$\begin{aligned} f_n &= \text{ the constant rate over a time step } [1/s] \\ \Delta t &= \text{ the length of a time step } [s]. \end{aligned}$$

In this model, at each time step, contaminants in the degraded fraction of the control volume are available for transfer to adjacent components such that,

$$m_{jk}(t_n) = m_{j,d}(t_n) \tag{10}$$

where

$$\begin{aligned} m_{jk}(t_n) &= \text{ incoming mass from the inner boundary } [kg] \\ m_{j,d} &= \text{ mass in degraded volume of cell j } [kg] \\ t_n &= \text{ time } [s]. \end{aligned}$$

The total contaminants $m_{j,d}(t_n)$, in the degraded volume at time t_n are calculated based on mass flux from the inner boundary, the updated mass in the degraded volume at the previous time step, and the mass released by degradation during the current time step. The contaminants in the degraded fluid (V_{df}) are effectively released in that barrier layer and can be transferred to the adjacent component in the mass transfer stage. Specifically,

$$m_{k,d}(t_n) = m_{jk}(t_n) + m^*_{k,d}(t_{n-1}) + m^*_{k,i}(t_{n-1}) f_n \Delta t \tag{11}$$

where

$$\begin{aligned} m^*_{k,d}(t_{n-1}) &= \text{ mass in the degraded volume of k at the end of } t_{n-1} \ [kg] \\ m^*_{k,i}(t_{n-1}) &= \text{ mass in the intact volume of k at the end of } t_{n-1} \ [kg] \\ f_n &= \text{ degradation rate during the time step } t_n \ [1/s] \\ \Delta t &= t_n - t_{n-1} \ [s]. \end{aligned}$$

The concentration calculation results from the mass balance calculation in (11) to support parent components that utilize the Dirichlet boundary condition. For the degradation rate model, which incorporates no diffusion or advection, the concentration, $C_j(r_j)$, the boundary (r_j) between cells j and k, is the average concentration throughout the degraded volume,

$$\begin{aligned} C_d &= \frac{m_d(t_n)}{V_d(t_n)} \\ &= \frac{\text{solute mass in degraded fluid in cell j}}{\text{degraded fluid volume in cell j}}. \end{aligned} \tag{12}$$

2.2.2. Mixed Cell Radionuclide Mass Balance Model

Slightly more complex, the Mixed Cell model incorporates the influence of porosity, elemental solubility limits, and sorption in addition to the degradation behavior of the Degradation Rate model. A graphical representation of the discrete sub-volumes in the mixed cell model is given in Figure 6.

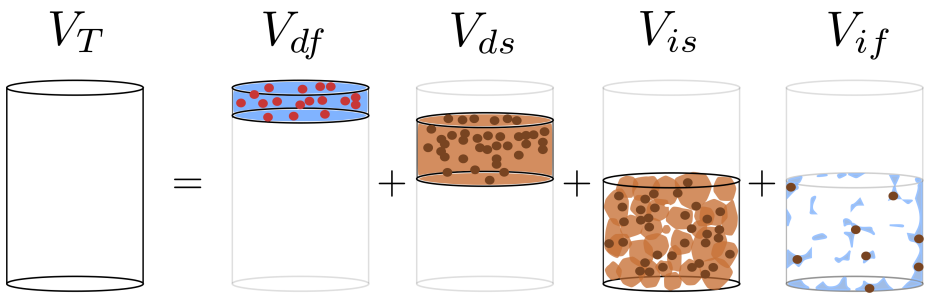

Figure 6: The degraded volume is modeled as a degraded solid volume, V_{ds}, and a degraded fluid volume, V_{df}. The intact volume is modeled as an intact solid volume, V_{is}, and an intact fluid volume V_{if}. Only contaminants in V_{df} are available for transport.

After some time degrading, the total volume in the degraded region (V_d) can be expressed as in equation (9). Additionally, given a volumetric porosity, θ, the

intact and degraded volumes can also be described in terms of their constituent solid matrix ($V_{is} + V_{ds}$) and pore fluid volumes ($V_{if} + V_{df}$),

$$\begin{aligned} V_d(t_n) = &\text{ degraded volume at time } t_n[m^3] \\ &= V_{df}(t_n) + V_{ds}(t_n) \end{aligned} \tag{13}$$

where

$$\begin{aligned} V_{df}(t_n) = &\text{ degraded fluid volume at time } t_n[m^3] \\ &= \theta V_d(t_n) \qquad (14) \\ &= \theta d(t_n) V_T \qquad (15) \end{aligned}$$

$$\begin{aligned} V_{ds}(t_n) = &\text{ degraded solid volume at time } t_n[m^3] \\ &= (1-\theta) V_d(t_n) \qquad (16) \\ &= (1-\theta) d(t_n) V_T \qquad (17) \end{aligned}$$

$$\begin{aligned} V_i(t_n) = &\text{ intact volume at time } t_n[m^3] \\ &= V_{if}(t_n) + V_{is}(t_n) \end{aligned} \tag{18}$$

$$\begin{aligned} V_{if}(t_n) = &\text{ intact fluid volume at time } t_n[m^3] \\ &= \theta V_i(t_n) \qquad (19) \\ &= \theta(1 - d(t_n)) V_T \qquad (20) \end{aligned}$$

and

$$\begin{aligned} V_{is}(t_n) = &\text{ intact solid volume at time } t_n[m^3] \\ &= (1-\theta) V_i(t_n) \qquad (21) \\ &= (1-\theta)(1 - d(t_n)) V_T. \qquad (22) \end{aligned}$$

This model distributes contaminant masses throughout each sub-volume of the component. Contaminant masses and concentrations can therefore be expressed with notation indicating in which volume they reside, such that

$$C_{df} = \frac{m_{df}}{V_{df}} \tag{23}$$

$$C_{ds} = \frac{m_{ds}}{V_{ds}} \tag{24}$$

$$C_{if} = \frac{m_{if}}{V_{if}} \tag{25}$$

$$C_{is} = \frac{m_{is}}{V_{is}}. \tag{26}$$

where

$$df = \text{degraded fluid} \tag{27}$$
$$ds = \text{degraded solid} \tag{28}$$
$$if = \text{intact fluid} \tag{29}$$
$$is = \text{intact solid.} \tag{30}$$

The contaminant mass in the degraded fluid (m_{df}) is the contaminant mass that is treated as "available" to adjacent components. That is, m_{df} is the mass vector m_{ij} which has been released by component i and can be transferred to component j in the following mass transfer phase.

Sorption. The mass in all volumes exists in both sorbed and non-sorbed phases. The relationship between the sorbed mass concentration in the solid phase (e.g. the pore walls),

$$s = \frac{\text{mass of sorbed contaminant}}{\text{mass of total solid phase}} \tag{31}$$

and the dissolved liquid concentration,

$$C = \frac{\text{mass of dissolved contaminant}}{\text{volume of total liquid phase}} \tag{32}$$

can be characterized by a sorption "isotherm" model. A sorption isotherm describes the equilibrium relationship between the amount of material bound to surfaces and the amount of material in the solution. The Mixed Cell mass balance model uses a linear isotherm model.

With the linear isotherm model, the mass of contaminant sorbed onto the solid phase, also referred to as the solid concentration, can be found [13], according to the relationship

$$s_p = K_{dp} C_p \tag{33}$$

where

$$\begin{aligned} s_p &= \text{ the solid concentration of isotope p } [kg/kg] \\ K_{dp} &= \text{ the distribution coefficient of isotope p}[m^3/kg] \\ C_p &= \text{ the liquid concentration of isotope p } [kg/m^3]. \end{aligned}$$

Thus, from (31),

$$\begin{aligned} s_{dsp} &= K_{dp} C_{dfp} \\ &= \frac{K_{dp} m_{dfp}}{V_{df}} \end{aligned}$$

where

$$\begin{aligned} s_{dsp} = &\text{ isotope p concentration in degraded solids } [kg/kg] \\ C_{dfp} = &\text{ isotope p concentration in degraded fluids } [kg/m^3]. \end{aligned}$$

In this model, sorption is taken into account throughout the volume. In the intact matrix, the contaminant mass is distributed between the pore walls and the pore fluid by sorption. So too, contaminant mass released from the intact matrix by degradation is distributed between dissolved mass in the free fluid and sorbed mass in the degraded and precipitated solids. Note that this model is agnostic to the mechanism of degradation. It simulates degradation purely from a rate and release is accordingly congruent [14] with that degradation.

To begin solving for the boundary conditions in this model, the amount of non-sorbed contaminant mass in the degraded fluid volume must be found. Dropping the isotope subscripts and beginning with equations (23) and (33),

$$m_{df} = C_{df} V_{df} \tag{34}$$

and assuming the sorbed material is in the degraded solids

$$m_{df} = \frac{s_{ds} V_{df}}{K_d},$$

then applying the definition of s_{ds} and m_{ds}

$$\begin{aligned} m_{df} &= \frac{\frac{m_{ds}}{m_T} V_{df}}{K_d} \\ &= \frac{(dm_T - m_{df}) V_{df}}{K_d m_T}. \end{aligned}$$

This can be rearranged to give

$$\begin{aligned} m_{df} &= \frac{dV_{df}}{K_d} \frac{1}{\left(1 + \frac{V_{df}}{K_d m_T}\right)} \\ &= \frac{dV_{df}}{\left(K_d + \frac{V_{df}}{m_T}\right)}. \end{aligned} \tag{35}$$

Finally, using the definition of V_{df} in terms of total volume,

$$m_{df} = \frac{d^2 \theta V_T}{K_d + \frac{d\theta V_T}{m_T}}. \tag{36}$$

Solubility. Dissolution of the contaminant into the available fluid volume is constrained by the elemental solubility limit. The reduced mobility of radionuclides with lower solubilities can be modeled [15] as a reduction in the amount of solute available for transport, thus:

$$m_i(t) \leq V(t) C_{sol,i} \tag{37}$$

where

$$\begin{aligned} m_i &= \text{ mass of isotope i in volume } V[kg] \\ V &= \text{ a distinct volume of fluid } [m^3] \\ C_{sol,i} &= \text{ the maximum concentration of i } [kg \cdot m^{-3}]. \end{aligned}$$

That is, the mass m_i in kg of a radionuclide i dissolved into the waste package void volume V_1 in m^3, at a time t, is limited by the solubility limit, the maximum concentration, C_{sol} in kg/m^3 at which that radionuclide is soluble [15].

The final available mass is therefore the m_{df} from equation (36) constrained by:

$$m_{df,i} \leq V_{df} C_{sol,i} \tag{38}$$

where

$$\begin{aligned} m_{df,i} &= \text{ solubility limited mass of isotope i in volume } V_{df}[kg] \\ C_{sol,i} &= \text{ the maximum dissolved concentration limit of i } [kg/m^3]. \end{aligned}$$

2.2.3. Lumped Parameter Radionuclide Mass Balance Model

For systems in which the flow is sufficiently slow to be assumed constant over a time step, it is possible to model a system of volumes as a connected lumped parameter models (Figure 7). The Lumped Parameter mass balance model implements a response function model based on this lumped parameter interpretation and capable of Piston Flow, Exponential, and Dispersion response functions from Maloszewski and Zuber [16].

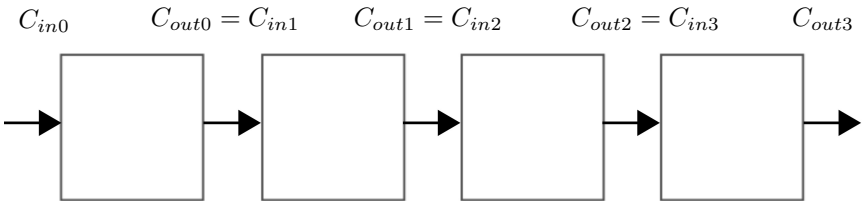

Figure 7: A system of volumes can be modeled as lumped parameter models in series.

Each lumped parameter component is modeled according to a relationship between the incoming concentration, $C_{in}(t)$, and the outgoing concentration, $C_{out}(t)$,

$$C_{out}(t) = \int_0^\infty C_{in}(t - t')g(t')e^{-\lambda t'}dt' \tag{39}$$

where

$$\begin{aligned} t' &= \text{ transit time } [s] \\ g(t') &= \text{ response function, a.k.a. transit time distribution}[-] \\ \lambda &= \text{ radioactive decay constant } [s^{-1}]. \end{aligned}$$

Selection of the response function is usually based on experimental tracer results in the medium at hand. If such detailed transport data is not available, functions used commonly in chemical engineering applications [16] include the Piston Flow Model (PFM), which approximates pure advection,

$$g_{PFM}(t') = \delta(t' - t_t)), \tag{40}$$

the Exponential Model (EM) which approximates a well-mixed flow case,

$$g_{EM}(t') = \frac{1}{t_t} e^{-\frac{t'}{t_t}} \tag{41}$$

and the so-called Dispersion Model (DM), which actually approximates the solution to both advective and dispersive transport,

$$g_{DM}(t') = \left(\frac{Pe\ t_t}{4\pi t'}\right)^{\frac{1}{2}} \frac{1}{t'} e^{-\frac{Pe\ t_t\left(1-\frac{t'}{t_t}\right)^2}{4t'}}, \tag{42}$$

where

$$\begin{aligned} Pe &= \text{ Peclet number for mass diffusion } [-] \\ t_t &= \text{ mean tracer age } [s] \\ &= t_w \text{ if there are no stagnant areas} \\ t_w &= \text{ mean residence time of water } [s] \\ &= \frac{V_m}{Q} \\ &= \frac{z}{v_z} \\ &= \frac{z\theta_e}{q} \end{aligned}$$

in which

$$\begin{aligned} V_m &= \text{ mobile water volume } [m^3] \\ Q &= \text{ volumetric flow rate } [m^3/s] \\ z &= \text{ average travel distance in flow direction } [m] \\ v_z &= \text{ mean water velocity} [m/s] \\ q &= \text{ Darcy Flux } [m/s] \\ \theta_e &= \text{ effective (connected) porosity } [\%]. \end{aligned}$$

The latter of these, the Dispersion Model satisfies the one dimensional advection-dispersion equation, and is therefore the most physically relevant for this application. A constant inlet concentration is assumed over the span of a time step such that $C_{in}(t) = C_0$, and the solutions to these for constant concentration at the source boundary are given in Maloszewski and Zuber [16] accordingly,

$$C_{out}(t) = \begin{cases} PFM & C_0 e^{-\lambda t_t} \\ EM & \frac{C_0}{1+\lambda t_t} \\ DM & C_0 e^{\frac{Pe}{2}\left(1-\sqrt{1+\frac{4\lambda t_t}{Pe}}\right)}. \end{cases} \tag{43}$$

Because Cyclus handles decay outside of Cyder, the use of these models relies on a reference transit time and decay constant supplied by the user. The behavior of the reference isotope, in this way, fully defines the behavior of all isotopes.

It is important to note that a linear concentration profile is assumed between the inlet and the outlet of a given component in Cyder,

$$C(z,t) = C_{in}(t) + \frac{C_{out}(t) - C_{in}(t)}{z_{out} - z_{in}}(z - z_{in}). \tag{44}$$

This is an approximation that could be improved by direct use of the response functions themselves, under a change of variables from time to length.

2.2.4. One Dimensional Permeable Porous Medium Radionuclide Mass Balance Model

The advection dispersion equation is at the core of contaminant transport. A description of advection and dispersion appears in the following section on mass transfer. For now, it is sufficient to note that various solutions to the advection dispersion equation (53) have been published for both the first and third types of boundary conditions. The third, Cauchy type, is more mass conservative, and is the primary kind of boundary condition used at the source for the model implementation in Cyder. Abstraction results informed modifications to the implementation of an analytic solution to the one dimensional

advection-dispersion equation with a finite domain and Cauchy and Neumann boundary conditions at the inner and outer boundaries, respectively.

The conceptual model in Figure 8 represents solute transport in one dimension with unidirectional flow upward and a finite boundary condition in the positive flow direction. Notably, unidirectional vertical flow upward in the far field simplifies a 3-dimensional problem into one dimenstion. The vertical direction was chosen to be conservative, since the shortest path to the biosphere is the vertical, z, direction. In CYCLUS, radioactive decay is handled external to the components, so there is no need to include production or decay. An approximate solution for these conditions made by Brenner [17] is described below as it is given in van Genuchten et. al, [18],

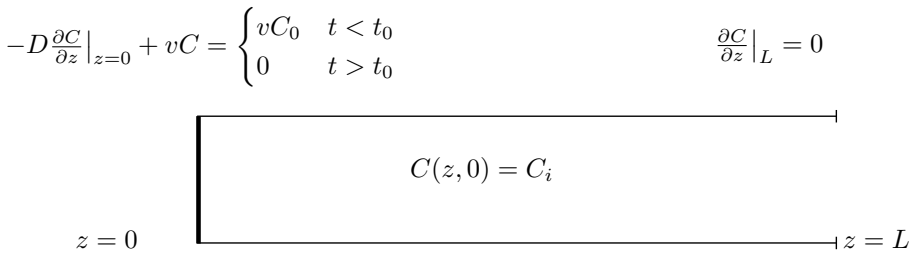

Figure 8: A one-dimensional, finite, unidirectional flow solution with Cauchy ($z = 0$) and Neumann ($z = L$) boundary conditions.

For the Cauchy boundary condition,

$$-D\frac{\partial C}{\partial z}\big|_{z=0} + v_z c = \begin{cases} v_z C_0 & (0 < t < t_0) \\ 0 & (t > t_0) \end{cases} \tag{45}$$

where

$$D = \text{ Effective Dispersion Coefficient } [m^2/s] \tag{46}$$
$$v = \text{ Fluid Velocity in the medium } [m/s] \tag{47}$$

the Neumann boundary condition,

$$\frac{\partial C}{\partial z}\big|_{z=L} = 0 \tag{48}$$

and the initial condition,

$$C(z,0) = C_i, \tag{49}$$

the solution is given as

$$C(z,t) = \begin{cases} C_i + (C_0 - C_i)\, A\,(z,t) & 0 < t \leq t_0 \\ C_i + (C_0 - C_i)\, A\,(z,t) - C_0 A(z, t - t_0) & t \geq t_0. \end{cases} \tag{50}$$

For the vertical flow coordinate system, A is defined as

$$\begin{aligned} A(z,t) = & \left(\frac{1}{2}\right) \operatorname{erfc}\left[\frac{Rz - vt}{2\sqrt{DRt}}\right] \\ & + \left(\frac{v^2 t}{\pi RD}\right)^{1/2} \exp\left[-\frac{(Rz - vt)^2}{4DRt}\right] \\ & - \frac{1}{2}\left(1 + \frac{vz}{D} + \frac{v^2 t}{DR}\right) \exp\left[\frac{vz}{D}\right] \operatorname{erfc}\left[\frac{Rz + vt}{2\sqrt{DRt}}\right] \\ & + \left(\frac{4v^2 t}{\pi RD}\right)^{1/2} \left[1 + \frac{v}{4D}\left(2L - z + \frac{vt}{R}\right)\right] \exp\left[\frac{vL}{D} - \frac{R}{4Dt}\left(2L - z + \frac{vt}{R}\right)^2\right] \\ & - \frac{v}{D}\left[2L - z + \frac{3vt}{2R} + \frac{v}{4D}\left(2L - z + \frac{vt}{R}\right)^2\right] \exp\left[\frac{vL}{D}\right] \operatorname{erfc}\left[\frac{R(2L - z) + vt}{2\sqrt{DRt}}\right] \end{aligned} \tag{51}$$

where

L =Extent of the solution domain $[m]$
R =Retardation factor $[-]$.

2.3. Mass Transfer Modes

The mass transfer interfaces between the mass balance models are essential to the understanding of the CYDER paradigm. Depending on the mass balance model selected in the external of two components, mass transfer into that component is either explicit or implicit.

In the explicit mode, the mass transfer mode is chosen by the user. Available options include advective, dispersive, coupled, or fixed flux. The corresponding transfer rate is calculated based on the conditions at the transfer boundary. The inventory in the components is then updated based on this transfer rate. While all components enable this on their outer boundary, only the mass balance models that are 0-dimensional in space (the Degradation Rate model and the Mixed Cell model) require explicit transfer on their inner boundary.

In the implicit mode, the mass balance model of the external component determines the inventory based on boundary conditions provided by the internal component. The appropriate mass is then transferred to accomplish the change in inventory.

In groundwater transport, contaminants are transported by dispersion and advection such that the mass conservation equation for mass flux becomes [13, 19, 18]:

$$J = J_{dis} + J_{adv} \tag{52}$$

where

$$\begin{aligned} J_{dis} &= \text{ Total Dispersive Mass Flux } [kg/m^2/s] \\ J_{adv} &= \text{ Advective Mass Flux } [kg/m^2/s]. \end{aligned}$$

It is customary to define the combination of molecular diffusion and mechanical mixing as the dispersion tensor, D, such that, for a conservative solute (infinitely soluble and non-sorbing), so that the dispersive component can be described in terms of the concentration profile:

$$\begin{aligned} J_{dis} &= \text{ Total Dispersive Mass Flux } [kg/m^2/s] \\ &= -\theta(D_{mdis} + \tau D_m)\nabla C \\ &= -\theta D \nabla C \end{aligned}$$

where

$$\begin{aligned} \theta &= \text{ Porosity } [-] \\ \tau &= \text{ Tortuosity } [-] \\ C &= \text{ Concentration } [kg/m^3] \\ D_m &= \text{ Molecular diffusion coefficient } [m^2/s] \\ D_{mdis} &= \text{ Coefficient of mechanical dispersivity} [m^2/s] \\ D &= \text{ Effective Dispersion Coefficient } [m^2/s]. \end{aligned}$$

Meanwhile, the advective mass flux depends on the concentration, the porosity of the medium, and the fluid velocity in that medium,

$$\begin{aligned} J_{adv} &= \text{ Advective Mass Flux } [kg/m^2/s] \\ &= \theta v C \\ v &= \text{ Fluid Velocity in the medium } [m/s]. \end{aligned}$$

For uniform flow in $\hat{k}$,

$$\begin{aligned} J = &\left(-\theta D_{xx}\frac{\partial C}{\partial x}\right)\hat{\imath} + \left(-\theta D_{yy}\frac{\partial C}{\partial y}\right)\hat{\jmath} \\ &+ \left(-\theta D_{zz}\frac{\partial C}{\partial z} + \theta v_z C\right)\hat{k}. \end{aligned} \tag{53}$$

Solutions to this equation can be categorized by their boundary conditions. Those boundary conditions serve as the interfaces between components in the CYDER library of nuclide transport models by way of advective, dispersive, coupled, and fixed fluxes. This is supported by implementation in which vertical

advective velocity, v_z, is uniform throughout the system and in which characteristic geologic and material parameters such as the dispersion coefficient are known for each component.

The mass transfer modes available in CYDER represent a range of boundary conditions. The following sections cover the mathematical models defining those that have been implemented and how they relate to the mass balance models in Section 2.2.

2.3.1. Explicit, Advection-Dominated Mass Transfer

Specified-concentration, or Dirichlet type, boundary conditions define a specified species concentration on some section of the boundary of the representative volume,

$$C(\vec{r},t)\Big|_{\vec{r}\in\Gamma} = C_0(t) \tag{54}$$

where

$$\begin{aligned}\vec{r} =&\ \text{position vector}\\ \Gamma =&\ \text{domain boundary .}\end{aligned}$$

The right hand side of the Dirichlet boundary condition can be provided by any mass balance model, j, at its external boundary, r_j, based on the concentration profile it calculates (see Section 2.2). The resulting concentration profile depends on the mass balance model chosen to represent that component,

$$\begin{aligned}C(z,t_n)|_{z=r_j} =&\ \text{fixed concentration in j at } r_j \text{ and } t_n[kg/m^3].\\ =&\begin{cases}\frac{m_d(t_n)}{V_d(t_n)}, & \text{Degradation Rate}\\ \frac{m_{df}(t_n)}{V_{df}(t_n)}, & \text{Mixed Cell}\\ C_{out}(t_n), & \text{Lumped Parameter}\\ C(r_j,t_n), & \text{One Dimensional PPM.}\end{cases}\end{aligned} \tag{55}$$

In the Degradation Rate and Mixed Cell models, the Dirichlet boundary condition can be chosen to enforce an advective flux on the inner boundary. This choice is appropriate when the user expects a primarily advective interface between two components. The advective flux across the boundary between two components j and k, relies on the fixed concentration Dirichlet boundary condition at the interface, provided by the internal component, thus

$$\begin{aligned}J_{adv}(t_n) =&\ \text{potential advective flux at } t_n[kg/m^2/s]\\ &= \theta v C(z,t_n).\end{aligned} \tag{56}$$

The resulting mass transfer into the component is, therefore,

$$m_{jk}(t_n) = A\Delta t \theta_k v C(z, t_n)|_{z=r_j} \tag{57}$$

where

$$\begin{aligned} A = &\text{ surface area normal to flow } [m^2] \\ \Delta t = &\text{ length of the time step } [s]. \end{aligned}$$

When mass transfer is dispersion-dominated, this model should not be used. Instead, the dispersion-dominated model is more appropriate.

2.3.2. Explicit, Dispersion-Dominated Mass Transfer

The second type, specified dispersive flux, or Neumann type boundary conditions describe a full set of concentration gradients at the boundary of the domain,

$$\begin{aligned} \frac{\partial C(\vec{r}, t)}{\partial r}\Big|_{\vec{r}\in\Gamma} &= f(t) \\ f(t) = &\text{ known function .} \end{aligned} \tag{58}$$

The Neumann boundary condition can be provided at the external boundary of any mass balance model,

$$\left.\frac{\partial C}{\partial z}\right|_{z=r_j} = \text{ concentration gradient at } r_j \text{ and } t_n [kg/m^3/s].$$

For mass balance models that are 0-dimensional in space (i.e. the Degradation Rate model and the Mixed Cell model), which lack spatial variation in the concentration profile, the differential must be approximated. Taking the center-to-center difference between adjacent components is one convenient way to make this approximation, and is the method implemented in CYDER, such that

$$\left.\frac{\partial C(z, t_n)}{\partial z}\right|_{z=r_j} = \frac{C_k(r_{k-1/2}, t_{n-1}) - C_j(r_{j-1/2}, t_n)}{r_{k-1/2} - r_{j-1/2}} \tag{59}$$

where

$$\begin{aligned} r_{j-1/2} &= r_j - \frac{r_j - r_i}{2} \\ r_{k-1/2} &= r_k - \frac{r_k - r_j}{2}. \end{aligned}$$

However, for mass balance models that are 1-dimensional in space (i.e. the Lumped Parameter model and the One Dimensional PPM model), the derivative

is taken based on the concentration profile in the internal component as it approaches the boundary. In component j, if it is a lumped parameter model, the profile is assumed to be a linear relationship between C_{in} and C_{out}, the gradient is

$$\left.\frac{\partial C(z,t_n)}{\partial z}\right|_{r_i \le z \le j} = \frac{C_{out} - C_{in}}{r_j - r_i}. \tag{60}$$

For the one dimensional permeable porous medium model, the analytical derivative of equation (51) is evaluated at r_j.

For mass transfer into the Degradation Rate and Mixed Cell models, the Neumann boundary condition can be chosen to enforce a dispersive flux on the inner boundary. This choice is appropriate when the user expects a primarily dispersive flow across the boundary. The dispersive flux in one dimension,

$$\begin{aligned} J_{dis} = &\text{ Total Dispersive Mass Flux } [kg/m^2/s] \\ &= -\theta D \frac{\partial C}{\partial z} \end{aligned}$$

relies on the fixed gradient Neumann boundary condition at the interface. The resulting mass transfer into the Degradation Rate or Mixed Cell model is, therefore,

$$m_{jk}(t_n) = -A\Delta t \theta_k D \frac{\partial C(z,t_n)}{\partial z}|_{z=r_j}. \tag{61}$$

If mass transfer is both advective and dispersive, a coupled model is available instead.

2.3.3. Explicit, Coupled, Advective-Dispersive Mass Transfer

The third Cauchy type mixed boundary condition defines a solute flux along a boundary. The fixed concentration flux Cauchy boundary condition can be provided at the external boundary of any mass balance model. For a vertically oriented system with advective velocity in the $\hat{k}$ direction,

$$-D\frac{\partial C(z,t)}{\partial z}\Big|_{z\in\Gamma} + v_z C(z,t) = v_z C(t) \tag{62}$$

where

$$C(t) = \text{ a known concentration function } [kg/m^3].$$

In the Degradation Rate and Mixed Cell models, the Cauchy boundary condition can be selected to enforce coupled advective and dispersive flow,

$$J_{coupled} = J_{adv} + J_{dis}$$
$$= \theta v C(z, t_n) - \theta D \frac{\partial C}{\partial z}. \tag{63}$$

The resulting mass transfer into the Degradation Rate or Mixed Cell model is then,

$$m_{jk}(t_n) = A\Delta t \theta_k \left(v C(z, t_n)\Big|_{z=r_j} - D \frac{\partial C(z, t_n)}{\partial z}\Big|_{z=r_j} \right). \tag{64}$$

2.3.4. Explicit, Maximum-Flow Mass Transfer

For debugging and testing purposes, the maximum flow mode transports all available material in a component into the component external to it.

The total available mass for each mass balance model can be expressed,

$$m_{jk}(t_n) = \begin{cases} m_{j,d}(t_n), & \text{Degradation Rate} \\ m_{j,df}(t_n), & \text{Mixed Cell} \\ \int C(z, t_n) dV_j, & \text{Lumped Parameter} \\ \int C(z, t_n) dV_j, & \text{One Dimensional PPM.} \end{cases} \tag{65}$$

The integrals for the Lumped Parameter model and the One Dimensional PPM model are calculated numerically.

2.3.5. Implicit Mass Transfer

On its inner boundary, the Lumped Parameter model uses the fixed concentration Dirichlet boundary condition directly in its solution such that,

$$C_{k,in}(t_n) = C(z, t_n)|_{z=r_j}. \tag{66}$$

The resulting mass transfer into the external component k containing the Lumped Parameter model is calculated by taking the integral of that concentration profile over the volume,

$$m_{jk}(t_n) = \int C(z, t_n) dV_k - \int C(z, t_{n-1}) dV_k. \tag{67}$$

In the similar case of the One Dimensional Permeable Porous Medium Model, the Dirichlet boundary condition at the boundary is also used directly in the solution as C_0 such that,

$$C_{k,0}(t_n) = C(z, t_n)|_{z=r_j}. \tag{68}$$

The mass transfer on the inner boundary is again calculated by taking an integral of that profile over the volume,

$$m_{jk}(t_n) = \int C(z, t_n) dV_k - \int C(z, t_{n-1}) dV_k. \tag{69}$$

3. Results and Discussion

In the present work, many numerical experiments successfully verified the CYDER software library. Multi-component simulations demonstrated expected transport behavior and the successful collective interaction of the modular components in a CYDER repository. Single-parameter sensitivity analyses demonstrated that physics captured by the CYDER models compare favorably to results reported in [20] from a more detailed existing model, the Clay GDSM, developed by the UFD Campaign within the DOE Office of Nuclear Energy [11].

In addition to these numerical experiments, a robust unit test suite was deployed during development to verify CYDER software implementation. Finally, CYDER was able to perform radionuclide transport calculations rapidly, on timescales of a few minutes rather than the timescales of a few hours seen in higher fidelity tools.

3.1. Multi-component Simulations

To verify the fundamental behavior of all four CYDER radionuclide transport models at each component interface, many transport and containment base cases were conducted.

The simulations were conducted within the CYCLUS framework and had the following simulation parameters:

- A 1000 year simulation
- A source facility providing one waste stream per time step
- An initial capacity of five 1 kg waste streams (in most cases)
- No more than one waste stream object is stored per waste form
- Corresponding waste package components, one per waste form
- A buffer component (i.e. a bentonite clay)
- A far field component (i.e. the host rock)

Each feasible combination of the four models was conducted to verify implementation of the time stepping algorithm and transport modes between components. A full description of each of these verification simulations can be found in the dissertation [21]. Among these simulations, one in which each component is represented with a Mixed Cell model is shown in Figures 9 through 13. The fixed maximum transport mode was used between mixed cell components for speed and clarity of results.

Solubility limitation is enabled in this case, so the system is expected to demonstrate solubility limited transport. To simultaneously demonstrate the behavior of the solubility limitation, no sorption is applied, but solubility limitation is set to 0.001 kg/m^3 for all isotopes. Please note that the CYDER user must currently provide reference solubility values for each isotope. While

this offers the user complete control, it may be inconvenient for some users. Future extensions to CYDER will include a default database for these values, perhaps through the Python toolkit for Nuclear Engineering (PyNE) database toolkit[22].

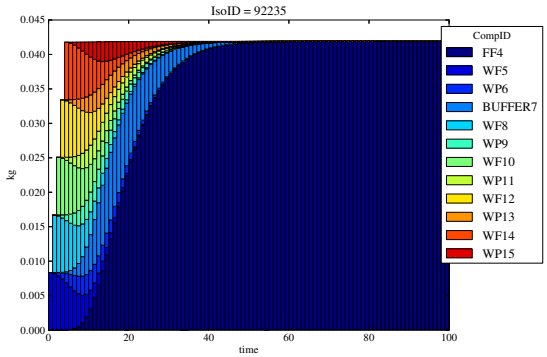

Figure 9: For the MCIII case in which containment is affected by solubility limitation, ($F_d = 0.1$ for all components except far field), ^{235}U travels through waste packages (WPN), their corresponding waste forms (WFN), and the surrounding buffer (BUFFER7) more slowly than in the MCI case before permanent residence in the far field component (FF).

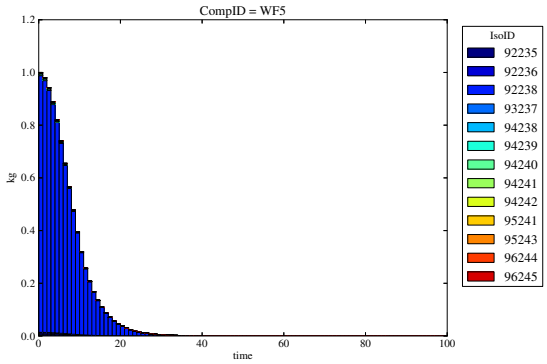

Figure 10: Waste Form 5 (degradation rate $F_d = 0.1[y^{-1}]$, reference solubility limit $S_{ref} = 0.001kg/m^3$) releases material with degradation.

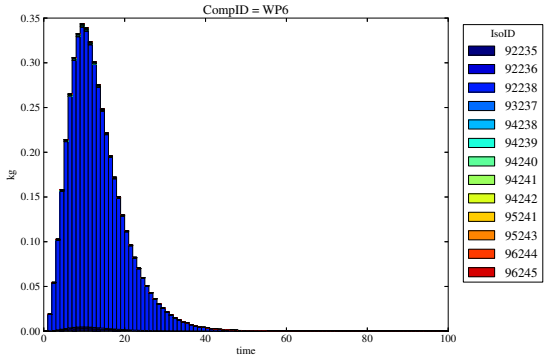

Figure 11: Waste Package 6 (degradation rate $F_d = 0.1[y^{-1}]$, reference solubility limit $S_{ref} = 0.001kg/m^3$) receives then releases material.

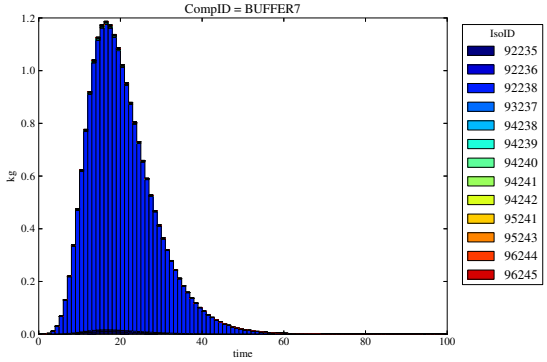

Figure 12: The Buffer, component 7 (degradation rate $F_d = 0.1[y^{-1}]$, reference solubility limit $S_{ref} = 0.001kg/m^3$), receives and then releases material.

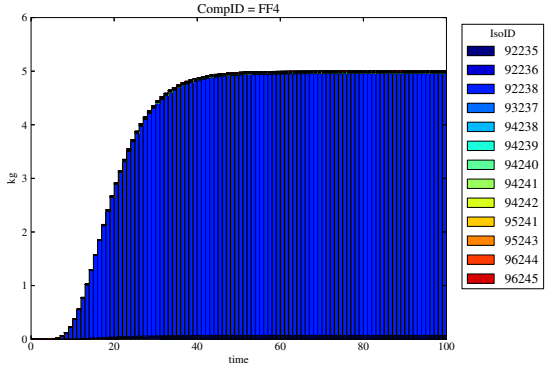

Figure 13: All material is released into the Far Field, component 4 (degradation rate $F_d = 0.0[y^{-1}]$, reference solubility limit $S_{ref} = 0.001kg/m^3$).

3.2. Single Effect Parametric Analyses

Each of the radionuclide contaminant transport models described in Section 2 capture different combintations of physics present in the hydrologic contaminant transport problem. To determine how effectively these physics were captured, single-effect simulations were conducted with CYDER and compared to similar analysis [20] conducted with a more detailed radionuclide transport model, the Clay GDSM [11]. The Clay GDSM was developed by the UFD Campaign within the DOE Office of Nuclear Energy using the GoldSim simulation environment [23]. Hydrologic contaminant transport in the Clay GDSM relies on the GoldSim contaminant transport module [12].

These single-effect sensitivity analyses were constructed by repeated multi-component simulation runs conducted across the valid range for a single parameter. To verify the behavior of a single parameter of each of the CYDER models, one hundred multi-component simulations were conducted, each with a different value of that parameter. This parametric analysis was conducted to show that, for an arbitrary isotope, the expected dependence on that parameter is captured. In the case of real isotopes in a full simulation, the same model will be invoked with real parameters for each isotope. Thus, the this model agreement is representative in all cases.

The results acheived with CYDER were compared to the results of a similiar parametric sensitivity analysis using the Clay GDSM which was reported in [20].

3.2.1. Solubility Sensitivity

To verify the behavior of the solubility limitation model in the Mixed Cell model, for example, one hundred multi-component simulations were conducted, each with a different reference solubility limit. For an arbitrary isotope, the expected solubility limitation behavior is captured and compared favorably to the Clay GDSM solubility limitation sensitivity results.

The results in Figure 14, from the detailed parametric analysis in [20], showed that for solubility limits below a certain threshold, the dose releases were directly proportional to the solubility limit, indicating that the radionuclide concentration saturated the groundwater up to the solubility limit near the waste form. For solubility limits above the threshold, however, further increase to the limit had no effect on the peak dose. This demonstrates the situation in which the solubility limit is so high that even complete dissolution of the waste inventory into the pore water is insufficient to reach the solubility limit.

In the corresponding parametric analysis of CYDER performance, it was shown that the solubility sensitivity behavior closely matched that of the GDSM sensitivity behaviors. Specifically, in Figure 15, a marked transition to the solubility-limited regime is seen where the solubility limit exceeds the point at which it limits movement. For increased solubility limits, release remains constant, as expected.

In both CYDER and the more detailed Clay GDSM, for solubility constants lower than the saturation threshold, the transport regime is solubility limited

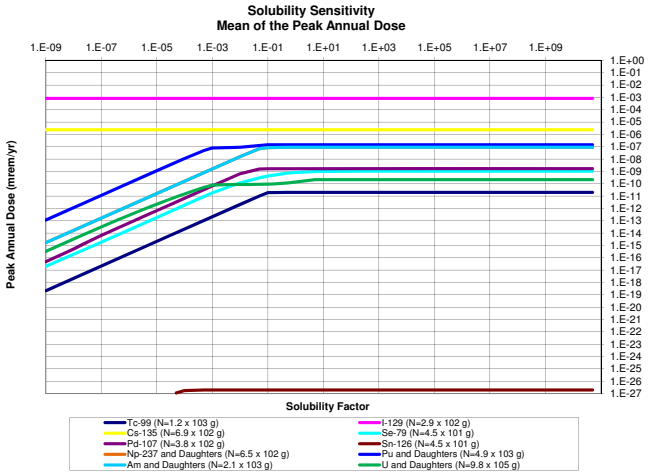

Figure 14: Solubility factor sensitivity in the DOE Clay GDSM, reproduced from [20]. The peak annual dose due to an inventory, N, of each isotope. This result was achieved with a parametric analysis using a detailed model of a generic clay repository.

and the relationship between peak annual dose and solubility limit is strong. Above the threshold, the transport regime is inventory limited instead.

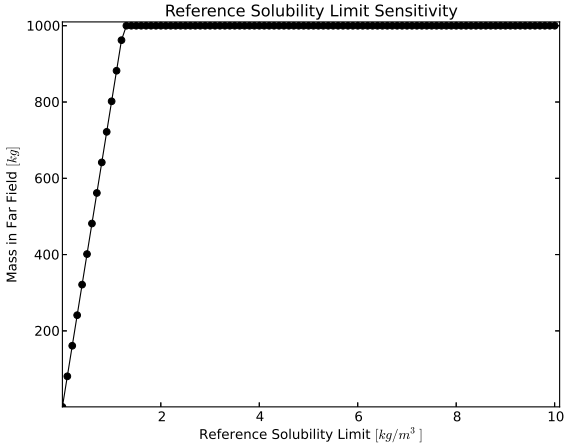

Figure 15: Sensitivity demonstration of solubility limitation in CYDER for an arbitrary isotope assigned a variable solubility limit.

3.2.2. Sorption Sensitivity

As the distribution coefficient K_d increases, so does the retardation coeffcient R_f, according to the relation $R_f = 1 + \rho_b \frac{K_d}{\theta}$. As these two values increase, contaminants tend toward the solid phase. An increase in these coefficients, then, has the effect of limiting dissolved concentration.

In the parametric sensitivity analysis reported in [20], the expected inverse relationship between the retardation factor and resulting peak annual dose was found for all elements except ^{129}I and ^{79}Se. These two isotopes have effectively no solubility limit and therefore demonstrate no sensitivity whatsoever to a the solubility limit multiplication factor. In the low retardation coefficient cases, a regime is established in which the peak annual dose is entirely unaffected by changes in retardation coefficient.

For large values of retardation coefficient, the sensitivity to small changes in the retardation coefficient increases dramatically. In that sensitive regime, the change in peak annual dose is inversely related to the retardation coefficient. Between these two regimes was a transition regime, in which the K_d factor ranges from 1×10^{-5} to $5 \times 10^{0}[-]$.

It is clear from Figure 16 that for retardation coefficients greater than a threshold, the relationship between peak annual dose and retardation coefficient is a strong inverse one.

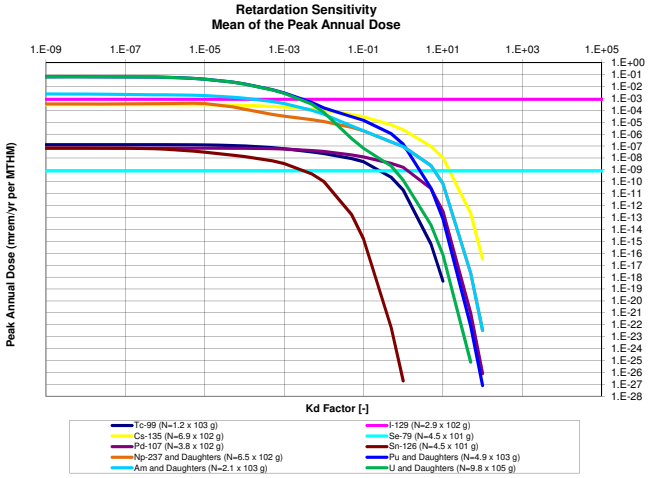

Figure 16: K_d factor sensitivity in DOE Clay GDSM, reproduced from [20]. The peak annual dose due to an inventory, N, of each isotope.

In the parametric analysis of CYDER performance, it was shown that sorption sensitivity behavior closely matched that of the GDSM sensitivity behaviors. Specifically, in Figure 17, increasing the retardation coefficient results in a smooth but dramatic turnover.

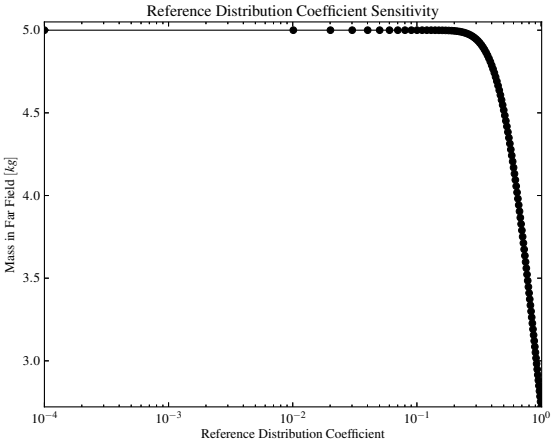

Figure 17: K_d sensitivity in the CYDER tool for an arbitrary isotope assigned a variable K_d coefficient.

3.2.3. Waste Form Degradation Rate Sensitivity

In the parametric sensitivity analysis reported in [20], the results showed two regimes. In the first regime, the mean of the peak annual dose rates is directly proportional to both the mass factor (an inventory mass multiplier) and the fractional waste form degradation rate. For some radionuclides, attenuation occurs for large values of both parameters as the release of radionuclides is limited by dispersion parameters. This phenomenon can be seen in the figures below in which transition between regimes for fast degradation rates occurs at smaller mass factors than does transition between regimes when the degradation rate is slow.

The peaks for highly soluble, non-sorbing elements such as I and Cl are directly proportional to mass factor for most values of waste form degradation rates. This effect can be seen in Figures 18 and 19.

Highly soluble and non-sorbing ^{129}I demonstrates a direct proportionality between dose rate and fractional degradation rate until a turnover where other natural system parameters dampen transport.

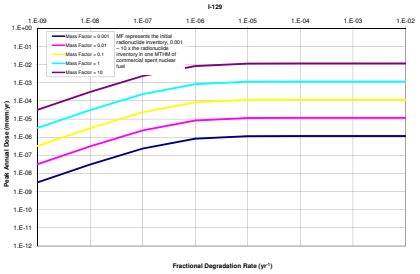

Figure 18: ^{129}I waste form degradation rate sensitivity demonstrated in Clay GDSM [20].

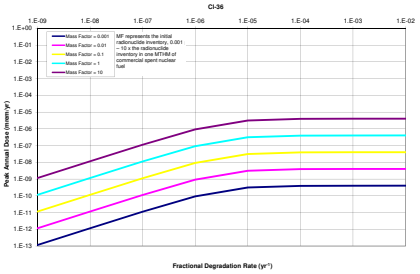

Figure 19: ^{36}Cl waste form degradation rate sensitivity demonstrated in Clay GDSM [20].

In the parametric sensitivity analysis conducted with the CYDER tool, waste form degradation rate sensitvity similarly shows the two regimes noted in the GDSM analysis.

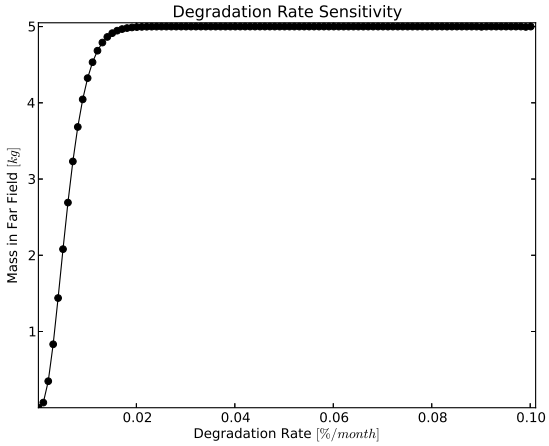

Figure 20: Sensitivity demonstration of the degradation rate in CYDER for an arbitrary isotope.

4. Conclusions

This paper has described the design, development, and verification of CYDER, a flexible software library for rapid medium-fidelity calculation of hydrologic contaminant transport integrated within a fuel cycle simulation library. In this work, four medium fidelity modeling methods for geologic radioactive waste disposal performance analysis were described as was their implementation in the CYDER repository performance library. This hydrologic nuclide transport library, by virtue of its capability to modularly integrate with the

CYCLUS fuel cycle simulator has demonstrated a new capability for integrated disposal options analysis when fuel cycle and nuclear waste disposal decisions are technologically coupled.

CYDER performance within the CYCLUS fuel cycle simulator and agreement between Cyder and the more detailed stand-alone GDSM model were also demonstrated. While CYDER methods make a strategic trade-off between speed and fidelity, they were shown to capture essential physics when computing back-end nuclear fuel cycle metrics. The result is a library of medium-fidelity hydrologic contaminant transport models within a disposal facility simulation framework appropriate for use in dynamic nuclear fuel cycle simulators.

Finally, this work contributes to an expanding ecosystem of computational models available for use with the CYCLUS fuel cycle simulator. Like those tools, the CYDER source code is freely available to interested researchers and potential model developers [9]. In addition to the source code and supporting publications, the CYDER library is well commented and produces clickable, browsable automated documentation with each build. That documentation is also available online.

5. Acknowledgements

This work was supported by the U.S. Department of Energy, Basic Energy Sciences, Office of Nuclear Energy, under contract # DE-AC02-06CH11357. This work was also supported by the Department of Energy National Nuclear Security Administration under Award Number DENA0000979 through the Nuclear Science and Security Consortium. Additionally, the author would like to acknowledge the support of advisors Professor Paul P.H. Wilson and Dr. W. Mark Nutt. Both were instrumental in arriving at modeling decisions for this software.

References

[1] M. Abkowitz, G. Rowe, N. Mote, B. Kirstein, Nuclear Waste Assessment System for Technical Evaluation (NUWASTE), in: Proceedings of the 2011 International High-Level Radioactive Waste Management Conference, American Nuclear Society, Albuquerque, NM, United States, 2011, pp. 10–14.
URL http://www.nwtrb.gov/staff/gr-ihlwmc.pdf

[2] L. Van Den Durpel, D. C. Wade, A. Yacout, DANESS: a system dynamics code for the holistic assessment of nuclear energy system strategies, Proceedings of the 2006 System Dynamics Conference.

[3] E. Schneider, M. Knebel, W. Schwenk-Ferrero, NFCSim Scenario Studies of German and European Reactor Fleets, Tech. rep., LA-UR-04-4911, Los Alamos National Laboratory (2004).

[4] R. Gregg, ORION v3.12 Results, Arlington, VA, United States, 2011.
URL http://www.nwtrb.gov/meetings/2011/june/gregg.pdf

[5] P. P. H. Wilson, Comparing Nuclear Fuel Cycle Options, A report for the Reactor & Fuel Cycle Technology Subcommittee of the Blue Ribbon Commission on America's Nuclear Future.
URL https://curie.ornl.gov/system/files/documents/not%20yet%20assigned/wilson.fuel_.cycle_.comparisons_final.pdf

[6] L. Boucher, F. A. Velarde, E. Gonzalez, B. W. Dixon, G. Edwards, G. Dick, K. Ono, International comparison for transition scenario codes involving COSI, DESAE, EVOLCODE, FAMILY and VISION, in: Actinide and Fission Product Partitioning and Transmutation, San Francisco, USA, 2010, p. 61, http://www.oecd-nea.org/pt/iempt11/documents/I-1_NEAbenchmark.pdf.
URL https://inis.iaea.org/search/search.aspx?orig_q=RN:44052619

[7] A. M. Yacout, J. J. Jacobson, G. E. Matthern, S. J. Piet, D. E. Shropshire, C. Laws, VISION Verifiable Fuel Cycle Simulation of Nuclear Fuel Cycle Dynamics, in: Waste Management Symposium, 2006.
URL http://www.inl.gov/technicalpublications/Documents/3394908.pdf

[8] T. E. Radel, Repository modeling for fuel cycle scenario analysis, M.S. Nuclear Engineering and Engineering Physics, University of Wisconsin – Madison, Madison, WI (2007).
URL https://search.library.wisc.edu/catalog/9910034845902121

[9] K. D. Huff, Cyder : A Generic Geology Repository Performance Library, University of Wisconsin Madison, Madison, WI, United States, 2013.
URL katyhuff.github.com/cyder

[10] P. P. H. Wilson, K. D. Huff, M. Gidden, R. Carlsen, Cyclus: A Nuclear Fuel Cycle Code from the University of Wisconsin Madison, 2012.
URL fuelcycle.org

[11] D. Clayton, G. Freeze, E. Hardin, W. M. Nutt, J. Birkholzer, H. Liu, S. Chu, Generic Disposal System Modeling - Fiscal Year 2011 Progress Report, Tech. Rep. FCRD-USED-2011-000184, U.S. Department of Energy, Sandia, NM (Aug. 2011).

[12] Golder Associates, GoldSim Contaminant Transport Module, version 6.0 Edition, GoldSim Technology Group, 2010.

[13] F. W. Schwartz, H. Zhang, Fundamentals of ground water, Environmental Geology 45 (2004) 1037–1038.

[14] D. Kawasaki, J. Ahn, P. L. Chambre, W. G. Halsey, Congruent release of long-lived radionuclides from multiple canister arrays, Nuclear technology 148 (2) (2004) 181 – 193.
URL http://epubs.ans.org.ezproxy.library.wisc.edu/?p=nt:148

[15] A. Hedin, Integrated analytic radionuclide transport model for a spent nuclear fuel repository in saturated fractured rock, Nuclear Technology 138 (2).
URL http://epubs.ans.org.proxy.uchicago.edu/download/?a=3287

[16] P. Maloszewski, A. Zuber, Lumped parameter models for the interpretation of environmental tracer data, Manual on mathematical models in isotope hydrology. IAEA-TECDOC-910 (1996) 9–59.

[17] H. Brenner, The diffusion model of longitudinal mixing in beds of finite length. Numerical values, Chemical Engineering Science 17 (4) (1962) 229–243. doi:10.1016/0009-2509(62)85002-7.
URL http://www.sciencedirect.com/science/article/pii/0009250962850027

[18] M. T. Van Genuchten, W. J. Alves, Analytical solutions of the one-dimensional convective-dispersive solute transport equation, Technical Bulletin 9 (1661).

[19] H. F. Wang, M. P. Anderson, Introduction to groundwater modeling, Academic Press, 1982.

[20] K. Huff, M. Nutt, Key Processes and Parameters in a Generic Clay Disposal System Model, in: Transactions of the American Nuclear Society, Vol. 107 of Environmental Sciences General, the American Nuclear Society, San Diego, CA, 2012, pp. 208–211.
URL http://epubs.ans.org/download/?a=14711

[21] K. D. Huff, An Integrated Used Fuel Disposition and Generic Repository Model for Fuel Cycle Analysis, Ph.D. thesis, THE UNIVERSITY OF WISCONSIN - MADISON (Oct. 2013).
URL http://gradworks.umi.com/35/92/3592735.html

[22] C. Bates, E. D. Biondo, K. D. Huff, K. Kiesling, A. M. Scopatz, PyNE Progress Report, in: Transactions of the American Nuclear Society, American Nuclear Society, Anaheim, CA, United States, 2014.

[23] Golder Associates, GoldSim Graphical Simulation Environment User's Guide, version 5.1 Edition, GoldSim Technology Group, 2010.